ChemComm

Accepted Manuscript

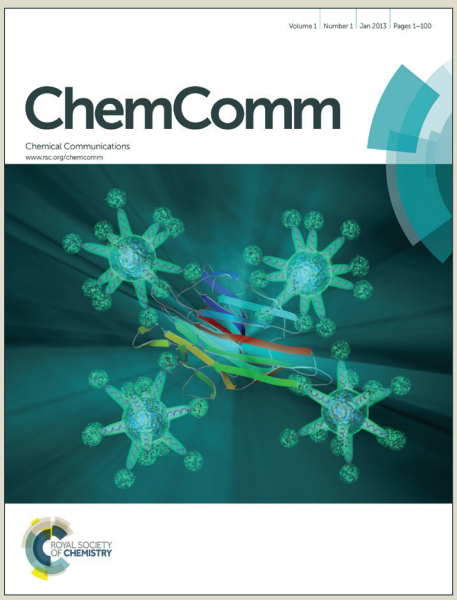

ROYAL SOCIETY OF CHEMISTRY

www.rsc.org/chemcomm

Cite this: DOI: 10.1039/c0xx00000x

www.rsc.org/xxxxxx

ARTICLE TYPE

Locked-Flavylium Fluorescent Dyes with Tunable Emission Wavelengths Based on Intramolecular Charge Transfer for Multi-color Ratiometric Fluorescence Imaging

Hua Chen, [b] Weiying Lin,*, [a, b] Wenqing Jiang, [b] Baoli Dong, [a] Haijun Cui, [b] and Yonghe Tang [a]

Received (in XXX, XXX) Xth XXXXXXXXX 20XX, Accepted Xth XXXXXXXXX 20XX
DOI: 10.1039/b000000x

A new type of locked-Flavylium fluorophores with tunable emission wavelengths based on intramolecular charge transfer were designed, synthesized, and evaluated. The optical studies indicate that the sensor LF3 can display an intriguing character, a fluorescence ratiometric response in three channels by tuning the ICT efficiencies.

Recently, fluorescence sensing has emerged as one of the most powerful techniques to monitor molecular targets and biological processes in the context of a living system.[1-3] In addition, by combining with fluorescence microscopy, fluorescence imaging can be employed to investigate biomolecules of interest with high temporal and spatial resolution.

Up to date, a large volume of fluorescent sensors have been developed. [4-5] However, most of them exhibit fluorescence signal variations only in one channel. [6] Since Terenin et al. reported the first example of dual fluorescence based on an excited-state intermolecular proton transfer (ESIPT) in 1947, [7] plenty of dyes have been reported to display dual fluorescence emission properties. Dual-channel based sensors have fluorescence signal changes in two distinct channels. This may reduce the potentials errors due to false positive signal from photobleaching or other environmental factors. [8] To this end, various molecular-design strategies based on intramolecular charge-transfer (ICT),[9] electronic energy-transfer, [10] excimer formation, [11] and ESIPT [12] have been exploited to construct a wide variety of dual-channel fluorescent sensors.

When compared to dual-channel fluorescent sensors, in principle, three-channel fluorescent sensors should be much more reliable to eliminate potential false positive or artifacts, as the fluorescent signals in three channels can be used for mutual corroboration. So far, a very few examples of fluorescent sensors based on the ESIPT strategy or traditional methods of mixing different primary emitting materials capable of showing three-channel fluorescence changes have been constructed.[3h,13] However, they only exhibit fluorescence OFF/ON response in three channels. To the best of our knowledge, sensors which can display a fluorescence ratiometric response in three channels have not been achieved yet.

Thus, how to design fluorescent sensors with such an intriguing feature became the focus of our attention. ICT is an effective signaling mechanism employed in design of ratiometric fluorescent sensors. Although, ICT-based sensors developed so far only show a fluorescence ratio response in two channels, we envisioned that, in principle, the ICT strategy could be exploited to design ratiometric three-channel fluorescent sensors.

Flavylium compounds are versatile molecules that comprise anthocyanins, the ubiquitous colorants used by nature to confer color to most flowers and fruits. They have found a wide range of applications from the millenary color paints to food additives. [14] Therefore, we decided to choose flavylium as the parent fluorescent core aiming to achieve a fluorescence ratiometric response in three channels based on an ICT process. Toward this end, we locked the flavylium backbone to prevent nonradiative decay affording a unique type of fluorescent dyes, named as **LF** dyes (Fig. 1). As shown in scheme S1, a series of **LF** dyes containing distinct substituents were readily synthesized in one step. For simplicity, the series of **LF** dyes are classified as three subtypes: **LF1** contains no hydroxyl group; **LF2** contains one hydroxyl group; **LF3** contains two hydroxyl groups (Fig. 1).

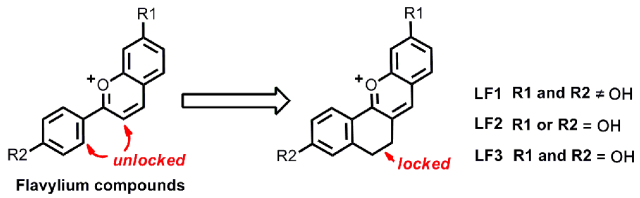

Fig. 1 Design of new **LF** dyes by locking the flavylium core.

With the compounds **LF** at hand, we then proceeded to investigate their optical properties in different solvents. The absorption and emission profiles of **LF** in distinct solvents (CH_2Cl_2 in the absence or presence of 1% HCl and PBS containing 1% CH_3CH_2OH) are shown in Fig. 2 and S1−3. In general, the flavylium cation is stable only at very acidic pH conditions.[14] Thus, we first investigated the spectral properties of **LF** dyes in aprotic solvent CH_2Cl_2 containing 1% HCl. **LF** dyes

exhibit strong fluorescence in a very acidic condition (Figure S1). For example, the emission peak of **LF1-3** is located at 518 nm, which is attributed to the cation form of **LF1-3** (Figure S1c and Scheme 1). To our surprise, in pure CH_2Cl_2 (in the absence of 1% HCl), the shape of emission spectra well resembles those in acidic conditions, indicating that locked-flavylium fluorescent dyes can also exist in the cation form in aprotic solvent CH_2Cl_2 (Figure S1 and Schemes 1 and S2).

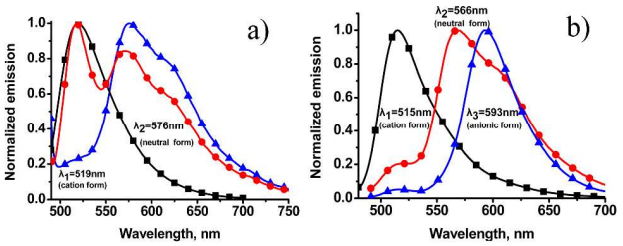

Fig. 2 The normalized fluorescence emission spectra of compounds **LF2-3** (a) at different pH values: pH=1(■), pH=5.5 (●) and pH=7.5 (▲); The normalized fluorescence emission spectra of **LF3** (b) at different pH values: pH=1(■), pH=5.5 (●) and pH=7.5 (▲).

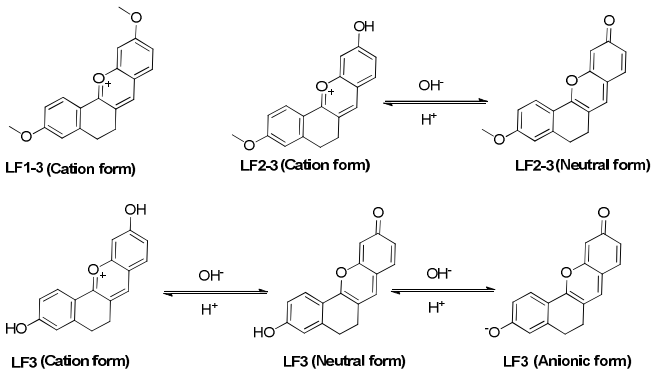

Scheme 1. Equilibria forms of **LF** dyes represented by **LF1-3**, **LF2-3** and **LF3**.

To get insight into the photophysical properties of new **LF** dyes, especially regarding how to tune the ICT efficiency through different equilibrium forms of **LF** dyes, we continue to test the spectral properties of these dyes in PBS containing 1% CH_3CH_2OH. Like in CH_2Cl_2 solutions, **LF2** dyes display only an emission band with the maximum wavelength at around 505-519 nm in a very acidic condition (pH = 1.0) (Figures 2 and S2). This emission band is also attributed to the cation form of **LF** dyes, which is similar with the phenomenon observed in CH_2Cl_2. **LF2** dyes change from the cation to neutral form with pH enhancement**,** accompanying with a redshift emission band with the maximum wavelength at around 552-576 nm. Interestingly, **LF3** have three equilibria forms at different pH values (Scheme 1). From the structure point of view, the ICT efficiency of **LF3** is in the order: the anionic form > the neutral form > the cation form. The improvement of ICT efficiency is usually accompanied by a redshift in emission and absorption. Thus, as expected, the maximum emission wavelength of three equilibria forms is in the order: 593 nm (the anionic form) > 566 nm (the neutral form) > 515 nm (the cation form) (Figure 2b). This absorption behavior of **LF3** dye is in good agreement with that of emission properties (Figure S3b).

To be useful as imaging agents in living systems, it is important that the novel **LF** dyes have sufficient photostability. The photostability of **LF** dyes in PBS is measured by continuous irradiation with a Xe lamp (150W) at 5 nm slit width at the corresponding maximal emission wavelength of **LF**, and the results demonstrate that over 95% of the initial fluorescence intensity is retained after 1 h irradiation (Figure S4), indicating that these functional dyes have sufficient photostability for potential biological imaging applications.

TD-DFT calculations are conducted to examine the potential effect of different equilibrium forms on the absorption and emission properties of novel **LF** dyes.[15] For example, **LF2-3** dye**,** the calculated emission peak of its neutral form is located at 574 nm, while its cation form is at 475 nm (Table S1). These data are well in accordance with the emission properties of the **LF2-3** in PBS (Figure 2a). For **LF3**, the absorption peak of its cation, neutral, and anionic forms is located at 439, 485, 515 nm, respectively (Table S1). Three equilibria forms of **LF3** have gradually increased ICT efficiency. With the increase of ICT efficiency, the absorption and emission wavelengths are gradually red shifted. Thus, these data are in good agreement with the photophysical properties of **LF3** in PBS (Figures 2 and S3b).

Biochemical processes frequently involve protonation and deprotonation of biomolecules with concomitant changes in the pH of the milieu. Protons are one of the most important targets among the intracellular species of interest.[16] **LF** dyes show unique properties of multiple emission bands in response to pH variations, which makes them ideal candidates for multi-color cellular imaging. For proof-of-concept, we applied **LF2-3** and **LF3** dyes as fluorescent sensors for dual-channel and three-channel pH detection, respectively.

First, we set out to investigate **LF2-3** dye as a potential fluorescent sensor for dual-channel pH detection, as the above spectral properties studies show that **LF2-3** can exist in two different equilibrium forms. The absorption and fluorescence spectra of **LF2-3** dye as a function of pH changes in aqueous solution are shown in Figures S5-6. As anticipated, **LF2-3** dye exhibits two main emission bands, intensities of which are pH dependent. Upon excitation at 470 nm, **LF2-3** displays a dramatic change in the emission profiles with 9.5- and 3.6-fold fluorescence intensity enhancements at the two emission channels at around 514 and 576 nm, respectively (Figure S5a and b). When excited at 520 nm, the emission band centered at 576 nm increases as the pH increases, and it shows a 9.9-fold fluorescence intensity enhancement (Figure S5c and d). As pH increases, the absorption band centered at 525 nm augments (Figure S6). This band is assigned to the neutral form of **LF2-3** (Scheme 1). At the same time, the absorption at ca. 476 nm decreases. The 460 nm band is assigned to the cation form of **LF2-3** (Scheme 1). The isosbestic point at 492 nm is observed (Figure S6). This isosbestic point is near the 488 nm Ar ion laser line. The pKa of compound **LF2-3** is calculated to be 4.50 based on the Henderson−Hasselbach-type mass action equation.[17]

According to the above spectral properties studies, **LF3** can

exist in three equilibrium forms with different ICT efficiencices to display three emission bands. This encourages us to examine the possibility of **LF3** as a fluorescent sensor for three-channel pH detection. As expected, upon excitation at 470 nm, **LF3** exhibits a significant change in the emission profiles in all three emission channels (Figure 3). The two emission bands at 515 and 566 nm decrease as the pH enhancement from 3.5 to 5.5, displaying a 31- and 3.54-fold fluorescence intensity changes at the two emission channels, respectively (Figure S7). As the pH increases from 5.5 to 8.5, the two emission channels centered at 515 and 566 nm decreases, while a new band centered at 595 nm enhances significantly (Figure 3). **LF3** shows large variations in two ratio modes (I_{593}/I_{566}, I_{593}/I_{515}) with pH enhancement. The ratio value (I_{593}/I_{566}) is changed from 0.70 to 3.96. Even more striking is that, another ratio value (I_{593}/I_{515}), is changed from 0.77 to 46.0 at the same time. To the best of our knowledge, this representes the first example of three-channel ratiometric fluorescent probe. The changes in the absorption profiles (Figure S8) are in good agreement with those in the emission. The pKa of **LF6** is calculated to be 4.30 and 6.82 based on the Henderson−Hasselbach-type mass action equation.[17]

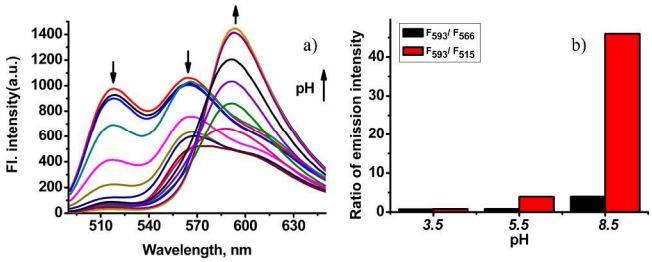

Fig. 3 a) pH-dependence of the fluorescence intensity of **LF3** (5 μM) with the arrow indicating the change of the fluorescence intensities with pH increase from 3.5 to 8.5, excitation at 470 nm; b) The emission ratio (I_{593}/I_{566}, I_{593}/I_{515}) of **LF3** at different pH values; Spectra were obtained in 25 mM PBS. The ratios of emission intensities at 593, 566, and 515 nm were measured.

Prompted by the above spectral studies, we then proceeded to investigate the feasibility of the sensor **LF2-3** for imaging pH in living cells. The standard MTT assays indicate that **LF2-3** and **LF3** have negligible cytotoxicity to living cells (Fig. S9). HeLa cells were incubated with sensor **LF2-3** (5μM) at 37 ºC for 30 min, and then the cells were washed in PBS medium of varying pH values with the addition of nigericin (1μg /mL) to elicit a rapid exchange of K^+ for H^+ for a fast equilibration of external and internal pH.[18] As shown in (Figure. S10), the cells treated with **LF2-3** in PBS (pH = 3.5) exhibit relatively strong fluorescence in the green and yellow channels. By contrast, when the cells pre-treated with PBS (pH = 4.5 or pH = 7.5), then incubated with **LF2-3**, the green channel gradually disappear, only the yellow channel is observed. These imaging data in living cells are consistent with the results in solution (Figure S5). HeLa cells were also incubated with sensor **LF2-3** (5μM) , and then the cells were washed in Britton-Robinson buffers medium of varying pH values with the addition of nigericin (1μg /mL) to elicit a rapid exchange of K^+ for H^+ for a fast equilibration of external and internal pH.[18] These imaging data in living cells are consistent with the results in PBS (Figure S11)

We then examined where probe LF3 is located in the living cells. HeLa cells were co-stained with the probe and LysoTracker green (a commercial lysosome probe) or Mitotracker green FM (a commercial mitochondrial probe), respectively. As shown in Fig. S12, the merged confocal fluorescence images of LF3 and commercial cellular organelle-specific probes did not overlap very well (Pearson's co-localization coefficient is 0.39 for lysosome and 0.43 for mitochondria, respectively.). These results suggest that the probe is not predominately located in these organelles, but in the cytoplasm.

Finally, we examined the possibility of the **LF3** sensor for multicolor ratiometric imaging of pH in living cells. The HeLa cells were incubated with the sensor **LF3** (5μM) at 37 ºC for 30 min, and then the cells were washed in PBS medium of varying pH values with the addition of nigericin (1μg /mL) to elicit a rapid exchange of K^+ for H^+ for a fast equilibration of external and internal pH.[18] With pH values increasing from 3.5 to 8.5, two ratio signal (F red / F green, F red / F yellow) augement significantly (Figure 4). These data establish that the sensor **LF3** is cell membrane permeable and can report pH changes in the living cells. Furthermore, this results of brightfield images imply that the cells are alive during the imaging experiments. The HeLa cells incubated with **LF3** in PBS (pH = 3.5) provide the average emission ratio values F_{red}/F_{green} and F_{red}/F_{yellow} at 5.8 and 4.9, respectively (Figure S12. By contrast, pH = 7.5, the average emission ratio values F_{red}/F_{green} and F_{red}/F_{yellow} are at 38.1 and 14.2 respectively (Figure S13). Thereby, these results indicate that **LF3** is capable of three-channel ratiometric fluorescent imaging of pH changes. To the best of our knowledge, this represents the first three-color ratiometric imaging of pH.

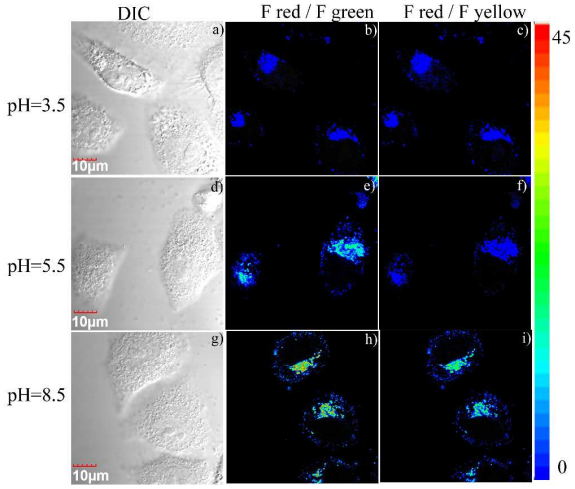

Fig. 4 *Pseudo*colored ratiometric images (F_{red} / F_{green}) and (F_{red} / F_{yellow}) of the HeLa cells stained with **LF3** at different pH values: (a–c) Brightfield and ratio images (F_{red} / F_{green}) and (F_{red} / F_{yellow}) of the cells incubated with **LF3** (5 μM) at pH = 3.5: (a) Brightfield image; (b) Ratio image (F_{red} / F_{green}); (c) Ratio image (F_{red} / F_{yellow}); (d–f) Brightfield and ratio images (F_{red} / F_{green}) and (F_{red} / F_{yellow}) of the cells incubated with **LF3** (5 μM) at pH = 5.5: (d) Brightfield image; (e) Ratio image (F_{red} / F_{green}); (f) Ratio image (F_{red} / F_{yellow}); (g–i) Brightfield and ratio image (F_{red} / F_{green}) and (F_{red} / F_{yellow}) of the cells incubated with **LF3** (5 μM) at pH=8.5: (g) Brightfield image; (h) Ratio image (F_{red} / F_{green}); (i) Ratio image (F_{red} / F_{yellow}). The green, yellow, and red channels are corresponding to the emission windows of 490-530, 540-580, and 580-640 nm, respectively. Scale bar =10 μm.

In summary, we have designed and synthesized a new type of locked-Flavylium fluorophores, **LF** dyes. The optical studies indicate that the sensor **LF3** can display a unique feature, a

fluorescence ratiometric response in three channels by tuning the ICT efficiencies. Furthermore, we have demonstrated that the sensor **LF3** is suitable for three-color ratiometric imaging of pH in living cells. We expect that the tuning ICT efficiency strategy can be applied to design various fluorescnt sensors for multi-color ratiometric imaging applications in living systems.

This work was financially supported by NSFC (21172063, 21472067) and the startup fund of University of Jinan.

Notes and references

[a] *Institute of Fluorescent Probes for Biological Imaging, School of Chemistry and Chemical Engineering, School of Biological Science and Technology, University of Jinan, Jinan, Shandong 250022, P.R. China. E-mail: Weiyinglin2013@163.com*

[b] *State Key Laboratory of Chemo/Biosensing and Chemometrics, College of Chemistry and Chemical Engineering, Hunan University, Changsha, Hunan 410082, China.*

† Electronic Supplementary Information (ESI) available: [details of any supplementary information available should be included here]. See DOI: 10.1039/b000000x/

1. (a) A. Hong-Hermesdorf, M. Miethke, S. D. Gallaher, J. Kropat, S. C. Dodani, J. Chan, S. S. Merchant, C. J. Chang, *Nat. Chem. Biol*., 2014, **10**, 1034; (b) Y. Qian, J. Karpus, O. Kabil, S.-Y. Zhang, H.-L. Zhu, R. Banerjee, J. Zhao, C. He, *Nat. Commun*., 2011, **2**, 495; (c) T. Liu, X. Liu, D. R. Spring, X. Qian, J. Cui, Z. Xu, *Scientific reports*, 2014, doi:10.1038/srep05418.
2. (a) A. P. de Silva, H. Q. N. Gunaratne, T. Gunnlaugsson, A. J. M. Huxley, C. P. McCoy, J. T. Rademacher, T. E. Rice, *Chem. Rev*., 1997, **97**, 1515; (b) S. Gnaim, D. Shabat, *Acc. Chem. Res*., 2014, **47**, 2970; (c) X. Li, X. Gao, W. Shi, H. Ma, *Chem. Rev*., 2014, **114**, 590; (d) Y. Yang, Q. Zhao, W. Feng, F. Li, *Chem. Rev*., 2013, **113**, 192.
3. (a) X. D. Wang, J. A. Stolwijk, T. Lang, M. Sperber, R. J. Meier, J. Wegener, O. S. Wolfbeis, *J. Am. Chem. Soc*., 2012, **134**, 17011; (b) J. C. Carlson, L. G. Meimetis, S. A. Hilderbrand, R. Weissleder, *Angew. Chem. Int. Ed*., 2013, **125**, 7055. (c) R. Tang, H. Lee, S. Achilefu, *J. Am. Chem. Soc.,* 2012, **134**, 4545; (d) L. Li, X. Shen, Q. H. Xu, S. Q. Yao, *Angew. Chem. Int. Ed*., 2013, **125**, 442; (e) W. Xuan, C. Sheng, Y. Cao, W. He, W. Wang, *Angew. Chem. Int. Ed*., 2012, **51**, 2282; (f) C. Huang, T. Jia, M. Tang, Q. Yin, W. Zhu, C. Zhang, X. Qian, *J. Am. Chem. Soc*., 2014, **136**, 14237; (g) H. Peng, Y. Cheng, C. Dai, A. L. King, B. L. Predmore, D. J. Lefer, B. Wang, *Angew. Chem. Int. Ed*., 2011, **50**, 1; (h) A. T. Wrobel, T.C. Johnstone, A. Deliz-Liang, S. J. Lippard, P. Rivera-Fuentes, *J. Am. Chem. Soc*., 2014, **136**, 4697; (i) T. Peng, N. K Wong, X. Chen, Y. K. Chan, D. H. H. Ho, Z. Sun, D. Yang, *J. Am. Chem. Soc*., 2014, **136**, 11728; (j) Y. J. Huang, W. J. Ouyang, X. Wu, Z. Li, J. S. Fossey, T. D. James, Y. B. Jiang, *J. Am. Chem. Soc*., 2013, **135**, 1700; (k) J. Liu, Y. Q. Sun, Y. Huo, H. Zhang, L. Wang, P. Zhang, W. Guo, *J. Am. Chem. Soc*., 2013, **136**, 574.
4. (a) Z. Guo, S. Park, J. Yoon, I. Shin, *Chem. Soc. Rev*., 2014, **43**, 16; (b) N. Boens, V. Leen, W. Dehaen, *Chem. Soc. Rev*., 2012, **41**, 1130; (c) Z. Yang, J. Cao, Y. He, J. H. Yang, T. Kim, X. Peng, J. S. Kim, *Chem. Soc. Rev*., 2014, **43**,4563.
5. (a) F. Hu, Y. Huang, G. Zhang, R. Zhao, H. Yang, D. Zhang, *Anal. Chem*. 2014, **86**, 7987; (b) S. Yang, Y. Qi, C. Liu, Y. Wang, Y. Zhao, L. Wang, J. Li, W. Tan. R. Yang, *Anal. Chem*. 2014, **86**, 7508; (c) G. Song, Y. Sun, Y. Liu, X. Wang, M. Chen, F. Miao, W. Zhang, X. Yu, J. Jin. *Biomaterials*, 2014, **35**, 2103; (d) T. Ozdemir, F. Sozmen, S. Mamur, T. Tekinay, E. U. Akkaya, *Chem. Commun*., 2014, **50**, 5455; (e) S. Ando, K. Koide, *J. Am. Chem. Soc*., 2011, **133**, 2556; (f) M. Abo, Y. Urano, K. Hanaoka, T. Terai, T. Komatsu, T. Nagano, *J. Am. Chem. Soc*., 2011, **133**, 10629; (g) X. F. Yang, Q. Huang, Y. Zhong, Z. Li, H. Li, M. Lowry, R. M. Strongin, *Chem. Sci*., 2014, **5**, 2177.
6. (a) Q. A. Best, N. Sattenapally, D. J. Dyer, C. N. Scott, M. E. McCarroll, *J. Am. Chem. Soc*., 2013, **135**, 13365; (b) H. Yu, Y. Xiao, L. Jin, *J. Am. Chem. Soc*., 2012, **134**, 17486; (c) S. Chang, X. Wu, Y. Li, D. Niu, Y .Gao, Z. Ma, W. Zhu, H. Tian, J. Shi, *Biomaterials*, 2013, **34**, 10182; (d) F. Yu, P. Li, B. Wang, K. Han, *J. Am. Chem. Soc*., 2011, **135**, 7674.
7. A. N. Terenin, A. Kariakin, *Nature*, 1947, **159**, 881.
8. (a) X. L. Liu, X. J. Du, C. G. Dai, Q. H. Song, *J. Org. Chem*., 2014, **79**, 9481; (b) M. Y. Wu, K. Li, C.Y. Li, J. T. Hou, X. Q.Yu, *Chem. Commun.,* 2014, **50**, 183; (c) B. Zhu, X. Zhang, Y. Li, P. Wang, H. Zhang, X. Zhuang, *Chem. Commun.,* 2010, **46**, 5710.
9. Z. R. Grabowski, K. Rotkiewicz, W. Rettig, *Chem. Rev*., 2003, **103**, 3899.
10. (a) L. Yuan, W. Lin, K. Zheng, S. Zhu, *Acc. Chem. Res*., 2013, **46**, 1462; (b) K. E. Sapsford, L. Berti, I. L. Medintz, *Angew. Chem. Int. Ed.,* 2006, **45**, 4562; (c) J. Han, J. Jose, E. Mei, K. Burgess, *Angew. Chem. Int. Ed*., 2007, **46**, 1684.
11. Z. Xu, N. J. Singh, J. Lim, J. Pan, H. N. Kim, S. Park, J. Yoon, *J. Am. Chem. Soc.,* 2009, **131**, 15528.
12. S. J. Lim, J. Seo, S.Y. Park, *J. Am. Chem. Soc*., 2006, **128**, 14542.
13. (a) J. Wang, W. Lin, W. Li, *Biomaterials,* 2013, **34**, 7429; (b) N. Li, C. Chang, W. Pan, B. Tang, *Angew. Chem. Int. Ed.,* 2012, **51**, 7426; (c) Y. Yang, M. Lowry, C. M. Schowalter, S. O. Fakayode, J. O .Escobedo, X. Xu, R. M. Strongin, *J. Am. Chem. Soc.,* 2006, **128**, 14081.
14. (a) F. Pina, *Dyes and Pigments,* 2014, **10**, 308; (b) F. Pin, M. J. Melo, C. A. T. Laia, A. J. Parola, J. C. Lima, *Chem. Soc. Rev*., 2012, **41**, 869.
15. M. J. Frisch, et al. GAUSSIAN 09 (Revision A.02), Gaussian, Inc.: Pittsburgh, PA, 2009.
16. (a) S. Chen, Y. Hong, Y. Liu, J. Liu, C. W. Leung, M. Li, B. Z. Tang, *J. Am. Chem. Soc*., 2013, **135**, 4926; (b) S. Wu, Z. Li, J. Han, S. Han, *Chem. Commun*., 2011, **47**, 11276; (c) R. Huang, S.Yan, X. Zheng, F. Luo, M. Deng, B. Fu, X. Zhou, *Analyst*. 2012, **137**, 4418.
17. The pKa was calculated according to the Henderson-Hasselbach-type mass action equation (log $[(F_{max} - F)/(F - F_{min})] = pK_a - pH$).
18. (a) E. Jähde, K.-H. Glüsenkamp, M.F. Rajewsky, *Cancer Chemother. Pharmacol*., 1991, **27** ,440; (b) M.E. Varnes, M.T. Bayne, G.R. Bright, *Photochem. Photobiol*., 1996, **64**, 853; (c) C. Y.-S. Chung, S. P.-Y. Li, M.-W. Louie, K. K.-W. Lob, V. W.-W. Yam, *Chem. Sci.*, 2013, **4**, 2453.